Nucleon Surface–Area Invariant in QMU: A Toroidal Ledger, Experiments, and Predictions for Particle Laboratories

David W. Thomson III *

James D. Bourassa

Quantum AetherDynamics Institute

September 18, 2025

Abstract

We present a two-parameter, thin-torus effective description of free nucleons in the Quantum Measurement Units (QMU) ledger: a conserved surface–area invariant σ (leng^2) and an aspect ratio Ξ. At low momentum transfer, electric, magnetic, and weak observables share the same geometry via operator-weighted moments $G_X(\hat{t}) = 1 - \hat{t}\,\rho_2^{(\mathrm{op})}/6 + \hat{t}^2\,\rho_4^{(\mathrm{op})}/120 + \cdots$, where $\rho_k^{(\mathrm{op})} = w_k^{(\mathrm{op})}(\zeta)\,\rho_k^{\mathrm{geom}}$ and $\rho_2^{\mathrm{geom}} = \sigma(\Xi + 2/\Xi)$, $\rho_4^{\mathrm{geom}} = \sigma^2(\Xi^2 + 6 + 3/\Xi^2)$. A single screened A_u Green kernel (fixed once on the proton) makes the framework predictive across channels and media. We highlight a falsifiable *neutron sign test*: $\mu_n < 0$ arises either from a helicity (topology) flip or from a shape node in the Canon $\xi(\Xi)$ bracket; parity-violating small-$\hat{t}$ data discriminate these cases. The program provides a QMU-only bridge to lattice/EFT slopes and spectroscopy, with closed-form radii retrieval, robust inversion from paired moments, and constant-area in-medium predictions. We include a complete, reproducible demonstration on a template proton-electric dataset that returns (σ, Ξ) and previews cross-channel predictions under illustrative operator weights.

1 Motivation, Axioms, and Relation to Established Frameworks

Motivation. We seek a *minimal* geometric reduction of nucleon observables into two dimensionless parameters (σ, Ξ) defined strictly in QMU, with hard falsifiers and lab-ready templates. The program is constructive: specify a small set of Canon axioms, derive operator-weighted moments at small $\hat{t}$, and pre-register predictions that survive cross-channel scrutiny. *Positioning.* We therefore invite the following reading: the Canon/QMU construction is a compact, falsifiable *parameterization tool* for the low-$\hat{t}$ regime where ab-initio QCD is expensive and EFT truncations compete. Its merit stands or falls on cross-channel consistency with a single (σ, Ξ) and a single kernel.

Canon axioms (APM/QMU).

A1 Aether Unit (A_u): an *operational, pre-geometric ledger* that fixes the base quantum length λ_C, quantum frequency F_q, and distributed charge capacities ${e_{emax}}^2$, ${e_{X\,\max}}^2$ that couple to surface currents.

*Email: david@quantumaetherdynamics.org; Corresponding author

A2 Leng^2 invariant: stable species realize thin toroidal surfaces with conserved $\sigma = \mathcal{R}\nabla$ in free space; binding deforms shape $\Xi = \mathcal{R}/\nabla$ at fixed σ.

A3 mchg scaling: ${e_{X\,\max}}^2/{e_{emax}}^2 = m_X/m_e$, implying $\chi_X = e^2/(8\pi {e_{X\,\max}}^2) = \alpha\, m_e/m_X$.

A4 Operator weighting (explicit): probes (electric, magnetic, weak) apply *channel weights* to the same geometry. Let

$$\rho_{2,X}^{\text{geom}} = \sigma_X\left(\Xi_X + \frac{2}{\Xi_X}\right), \qquad \rho_{4,X}^{\text{geom}} = {\sigma_X}^2\left({\Xi_X}^2 + 6 + \frac{3}{{\Xi_X}^2}\right).$$

For operator channel op $\in \{E, M, Z\}$,

$$\rho_{2,X}^{(\text{op})} = w_2^{(\text{op})}(\zeta)\,\rho_{2,X}^{\text{geom}}, \qquad \rho_{4,X}^{(\text{op})} = w_4^{(\text{op})}(\zeta)\,\rho_{4,X}^{\text{geom}}, \tag{1}$$

with dimensionless weights $w_k^{(\text{op})}$ fixed once the A_u kernel (screening ζ) is fixed. We adopt the *normalization convention* $w_2^{(E)} = w_4^{(E)} = 1$ on the proton electric channel; $w_k^{(M)}, w_k^{(Z)}$ are then determined (no new freedom). *Throughout, "moments" entering data fits are the operator-projected ones $\rho_k^{(\text{op})}$; geometric radii belong to ρ_k^{geom} and are obtained by $\rho_k^{\text{geom}} = \rho_k^{(\text{op})}/w_k^{(\text{op})}(\zeta)$ once the kernel is fixed.*[1]

Relation to QFT/GR and to QCD/EFT (bridge first). We treat the toroidal ledger as a *low-momentum effective theory* for nucleon observables. The construction is agnostic to point-like quark–gluon microphysics: it asserts that the *emergent, long-range* structure of the bound state dominates small-$\hat{t}$ data and possesses the symmetries of a thin surface with conserved area. In this reading, the A_u Green kernel is a long-distance propagator that is fixed *once* on the proton and then held for all other channels and media. Sections 4.1–6 give a concrete, testable map between QMU moments and lattice/EFT slopes and curvatures at small $\hat{t}$.

Table 1: Parameter roadmap (QMU/Canon). All inputs/outputs are dimensionless in QMU.

Parameter	Description	Determined by
ζ	A_u Green-kernel screening	Proton operator ratio ${\mathcal{R}_2}^{(p)} = \rho_{2,p}^{(E)}/\rho_{2,p}^{(M)}$
$k\,\tilde{I}_0$	Circulation quantum × current unit	Proton magnetic moment μ_p with (σ_p, Ξ_p)
σ_X, Ξ_X	Geometric invariants (area, shape)	Small-$\hat{t}$ slopes/curvatures (Prongs A, A′)
κ_X	Packing/organization efficiency	$\sigma_X = (8\pi\chi_X)^2\,\kappa_X$ (Sec. 4.1)
$w_k^{(\text{op})}(\zeta)$	Operator weights ($k = 2, 4$)	Fixed once by ζ (App. C)

[1] **Origin of operator weights.** In Canon, small-$\hat{t}$ slopes/curvatures are quadratic functionals of the *same* A_u Green kernel contracted with channel-specific source tensors (electric charge density, magnetic surface current, or weak neutral current). In the thin-surface limit this yields dimensionless prefactors $\mathcal{C}_k^{(\text{op})}(\zeta)$ ($k = 2, 4$) multiplying the geometric moments, so that $w_k^{(\text{op})}(\zeta) = \mathcal{C}_k^{(\text{op})}(\zeta)/\mathcal{C}_k^{(E)}(\zeta)$ under the proton-electric normalization $w_k^{(E)} = 1$. Thus $w_k^{(\text{op})}$ depend only on the *chosen* A_u screening ζ and on the operator's tensor structure, not on SI couplings; no extra fit parameters are introduced once the kernel is fixed. Intuitively, E vs. M vs. Z channels correspond to different linear combinations of the same toroidal/poloidal geometry kernels, reweighting the shared surface while leaving (σ, Ξ) unchanged.

2 Foundations: Aether Units and QMU Ledger

Definition and role of the Aether Unit. The Aether Unit is a *dimensionless* Canon/QMU combination that normalizes the vector-potential ledger and fixes the relative scale of length, frequency, and magnetic-charge capacity:

$$A_{\mathrm{u}} \;\equiv\; \frac{m_e\,{\lambda_C}^3\,{F_q}^2}{{e_{emax}}^2}. \tag{2}$$

It appears implicitly in the kernel normalization and in the circulation quantization (App. B); once the kernel (screening ζ) is fixed on the proton, A_u needs no separate calibration.

Aether unit geometry and distributed charge. In QMU, electrostatic charge appears as e^2 and the magnetic-charge capacities as ${e_{emax}}^2$ (electron), ${e_{pmax}}^2$ (proton), and ${e_{nmax}}^2$ (neutron) defined by Canon, with ${e_{pmax}}^2 \equiv {e_{pmax}}^2$. The Aether unit fixes a pre-geometric ledger with the base quantum length λ_C and quantum frequency F_q, along with electron mass m_e. The dimensionless charge-capacity ratio and nucleon fine-structures are

$$\eta_c \;\equiv\; \frac{e^2}{{e_{emax}}^2} = 8\pi\,\alpha, \qquad p \equiv \frac{e^2}{8\pi\,{e_{pmax}}^2}, \quad n \equiv \frac{e^2}{8\pi\,{e_{nmax}}^2}. \tag{3}$$

APM's mass–magnetic-charge scaling gives

$$\frac{{e_{pmax}}^2}{{e_{emax}}^2} = \frac{m_p}{m_e}, \qquad \frac{{e_{nmax}}^2}{{e_{emax}}^2} = \frac{m_n}{m_e}, \qquad \Rightarrow \qquad p = \alpha\frac{m_e}{m_p}, \quad n = \alpha\frac{m_e}{m_n}. \tag{4}$$

No SI and no Q. All observables are cast in QMU-only quantities. We avoid the Standard-Model Q^2 notation and define the *dimensionless* momentum variable

$$\hat{t} \;\equiv\; {\lambda_C}^2(-t), \tag{5}$$

where t is the Mandelstam variable. Experimental inputs are thus $(\hat{t},\, G(\hat{t}))$ without SI intermediaries.

3 Toroidal Geometry and Area Invariants (Proton and Neutron)

For each nucleon $X \in \{p, n\}$ we use the dimensionless radii

$$\mathcal{R}_X \equiv \frac{R_X}{\lambda_C}, \qquad \nabla_X \equiv \frac{r_X}{\lambda_C}, \qquad \Xi_X \equiv \frac{\mathcal{R}_X}{\nabla_X}, \tag{6}$$

and define the surface–area invariant (leng^2)

$$S_X = 4\pi^2 R_X r_X = 4\pi^2 {\lambda_C}^2\,\sigma_X, \qquad \sigma_X \equiv \mathcal{R}_X\,\nabla_X. \tag{7}$$

Species closure via fine-structure reads

$$\boxed{\sigma_p = \kappa_p(8\pi p)^2, \qquad \sigma_n = \kappa_n(8\pi n)^2}. \tag{8}$$

A *universal* $\kappa_p \approx \kappa_n$ implies $\sigma_n/\sigma_p \simeq (m_p/m_n)^2 \approx 1$.

Energetic definition and bounds for κ. At fixed χ_X and helicity k, define κ_X as the dimensionless proportionality between the A_u-minimizing surface area σ_X and $(8\pi\chi_X)^2$:

$$\kappa_X \equiv \frac{{\sigma_X}^{(\mathrm{gs})}}{(8\pi\chi_X)^2}, \qquad {\sigma_X}^{(\mathrm{gs})} = \arg\min_{\sigma,\ \Xi\geq 1} \mathcal{U}_{\mathrm{A_u}}[\sigma, \Xi; \zeta, k],$$

with $\mathcal{U}_{\mathrm{A_u}}$ the Canon self-energy functional (Appendix B, Eq. (36)). This variational definition supplies:

- a **lower bound** $\kappa_X \geq \kappa_{\min}(\zeta, k)$ from the discriminant $\rho_2^2 \geq 8\sigma^2$ and the $\Xi = \sqrt{2}$ minimum;
- an **isospin prior** $\kappa_n/\kappa_p = 1 + \delta_{\mathrm{iso}}$ with $|\delta_{\mathrm{iso}}| \ll 1$ in the isospin-symmetric limit of the same A_u kernel and helicity sector;
- a **measurable ratio** $\kappa_n/\kappa_p = (\sigma_n/\sigma_p)\,(p/n)^2$ (QMU-only).

Hence κ is not a free "efficiency," but the outcome of an A_u energy minimum subject to mchg and helicity constraints; differences between proton and neutron appear as controlled departures from isospin symmetry.

4 Low-$\hat{t}$ Form-Factor Templates (Operator-Weighted)

For a thin, uniformly charged surface, the geometric moments are

$$\rho_{2X} = {\mathcal{R}_X}^2 + 2{\nabla_X}^2 = \sigma_X\left(\Xi_X + \frac{2}{\Xi_X}\right), \tag{9}$$

$$\rho_{4X} = {\mathcal{R}_X}^4 + 6{\mathcal{R}_X}^2{\nabla_X}^2 + 3{\nabla_X}^4 = {\sigma_X}^2\left({\Xi_X}^2 + 6 + \frac{3}{{\Xi_X}^2}\right). \tag{10}$$

These moments control the small-$\hat{t}$ expansion of the appropriate Sachs form factor:

$$G_X(\hat{t}) = 1 - \frac{\hat{t}}{6}\,\rho_{2X} + \frac{\hat{t}^2}{120}\,\rho_{4X} + \mathcal{O}(\hat{t}^3), \tag{11}$$

with $G_p \to {G_E}^p$ (electric) and for the neutron either $G_n \to {G_M}^n$ (magnetic) or a weak analog ${G_E}^Z$ at small $\hat{t}$ (parity-violating channel). *Operator domain:* changing the probe (electric ${G_E}^p$, magnetic ${G_M}^n$, weak ${G_E}^Z$) changes only the *weights* applied to the same geometric moments $\{\rho_{2X}, \rho_{4X}\}$, not the underlying toroidal surface (σ_X, Ξ_X).

Operator weights made concrete. The small-$\hat{t}$ expansion in (11) uses the *operator-projected* moments $\rho_{2,4}^{(\mathrm{op})}$, not the raw geometric ones. With (1),

$$G_X^{(\mathrm{op})}(\hat{t}) = 1 - \frac{\hat{t}}{6}\,w_2^{(\mathrm{op})}\,\rho_{2,X}^{\mathrm{geom}} + \frac{\hat{t}^2}{120}\,w_4^{(\mathrm{op})}\,\rho_{4,X}^{\mathrm{geom}} + \mathcal{O}(\hat{t}^3).$$

Given the kernel choice (screening ζ) and our proton-electric normalization $w_{2,4}^{(E)} = 1$, the weights $w_k^{(M)}(\zeta)$ and $w_k^{(Z)}(\zeta)$ are fixed numbers (tabulated once; see App. C). This preserves the "same geometry, different weights" principle and avoids the unintended claim that all channels measure identical moments.

Reality & falsifiability bound. Solving for ${\mathcal{R}_X}^2$ yields the discriminant condition

$$\boxed{\left(\rho_{2,X}^{\mathrm{geom}}\right)^2 \geq 8\,{\sigma_X}^2} \quad \Longleftrightarrow \quad \left(\Xi_X + \frac{2}{\Xi_X}\right)^2 \geq 8 \quad \text{(equality at } \Xi_X = \sqrt{2}\text{)}. \tag{12}$$

Radii extraction from $\{\rho_{2,X}^{\mathrm{geom}}, \sigma_X\}$. To convert experimental/operator slopes to geometry, first divide out the weight: $\rho_{2,X}^{\mathrm{geom}} = \rho_{2,X}^{(\mathrm{op})}/w_2^{(\mathrm{op})}(\zeta)$. Then

$${\mathcal{R}_X}^2 = \frac{\rho_{2,X}^{\mathrm{geom}} \pm \sqrt{\left(\rho_{2,X}^{\mathrm{geom}}\right)^2 - 8{\sigma_X}^2}}{2}, \qquad {\nabla_X}^2 = \frac{{\sigma_X}^2}{{\mathcal{R}_X}^2}. \tag{13}$$

selecting the branch with $\mathcal{R}_X \geq \nabla_X$ (i.e., $\Xi_X \geq 1$). The equal-area spherical radius is

$$\boxed{\frac{a_X}{\lambda_C} = \sqrt{\pi\,\sigma_X} = \sqrt{\pi\,\kappa_X}\,(8\pi\,\chi_X)}, \qquad \chi_X \in \{p, n\}. \tag{14}$$

Robust moment inversion. Define $r_X \equiv \rho_{4X}/{\rho_{2X}}^2 = [{\Xi_X}^2 + 6 + 3/{\Xi_X}^2]/(\Xi_X + 2/\Xi_X)^2$. Protocol: (i) solve $r_X = r_X(\Xi_X)$ for $\Xi_X \geq 1$ numerically (minimum at $\Xi_X = \sqrt{2}$); (ii) set $\sigma_X = \rho_{2X}/(\Xi_X + 2/\Xi_X)$; (iii) recover $\mathcal{R}_X, \nabla_X$ via (13). This enforces (12) by construction.

4.1 A_u Green kernel specification

To close the Canon system, we fix the A_u vector-potential Green kernel $\mathcal{G}$ as the inverse of the A_u Laplace–screen operator,

$$(\nabla^2 - \zeta^2)\,\mathcal{G}(\boldsymbol{u}) = -\delta^{(3)}(\boldsymbol{u}), \qquad \boldsymbol{u} \equiv \boldsymbol{r}/\lambda_C,$$

with the *dimensionless* screening $\zeta \geq 0$. Thus $\mathcal{G}(u) = \exp(-\zeta u)/(4\pi u)$, recovering the unscreened Coulomb-like kernel at $\zeta \to 0$. We *determine* ζ *once* by a proton-only calibration under the pre-registered constraints (Prong A: small-$\hat{t}$ stability, TPE robustness), and *hold it fixed* for neutron and in-medium analyses. The geometry kernels $\ell_{\phi\phi}, \ell_{\theta\theta}, \ell_{\phi\theta}$ are then *unique* functions of Ξ and ζ (Appendix C), removing any ad-hoc freedom. *Physical motivation.* A Yukawa-like screening $\zeta > 0$ models a finite correlation length of the organizing currents on the thin surface (effective range of the binding environment). Fixing ζ once on the proton suppresses spurious long-range sensitivity and makes cross-channel predictions rigid while retaining the correct Coulomb-like limit as $\zeta \to 0$.

5 Spectroscopy in QMU and Cross-Checks

Hydrogenic nS finite-size frequency shift in QMU units (electric operator):

$$\frac{\Delta f_{\mathrm{fs}}(nS)}{F_q} = \frac{2}{3}\,\alpha^4\,\frac{\hat{\mu}^3}{n^3}\;\rho_{2p} = \frac{2}{3}\,\alpha^4\,\frac{\hat{\mu}^3}{n^3}\;\sigma_p\left(\Xi_p + \frac{2}{\Xi_p}\right), \tag{15}$$

with $\hat{\mu} = m_r/m_e$. For neutron-sensitive weak transitions in nuclei, replace ρ_{2p} by the appropriate weak-weighted ${\rho_{2n}}^{(Z)}$ built from $\{\sigma_n, \Xi_n\}$ and the same geometry.

6 Benchmark Bridge to QCD/EFT at Small $\hat{t}$

Scope. We compare *operator-specific slopes/curvatures* at small $\hat{t}$, where EFT and lattice computations report moments, without importing SI into Canon.

Observable map (QMU ↔ mainstream notations). Let ${\langle r^2\rangle_{E,M}}^X$ denote the traditional mean-square radii. Our Canon moments satisfy

$$\frac{d{G_E}^p}{d\hat{t}}\Big|_0 = -\frac{\rho_{2p}}{6}, \quad \frac{d{G_M}^n}{d\hat{t}}\Big|_0 = -\frac{{\rho_{2n}}^{(M)}}{6}, \quad \frac{d{G_E}^Z}{d\hat{t}}\Big|_0 = -\frac{{\rho_{2n}}^{(Z)}}{6},$$

so any lattice/EFT report of small-t slopes translates into ρ_2 directly (and similarly for ρ_4 with the 1/120 coefficient). The *geometry* (σ, Ξ) then follows from Sec. 4.

Bridge hypothesis (falsifiable). We hypothesize that long-distance nucleon structure is captured by a thin-surface A_u geometry, such that lattice/EFT slopes obey the Canon bound ${\rho_2}^2 \geq 8\sigma^2$ and are jointly fit by (σ, Ξ) *with a single* A_u *kernel* ζ fixed on the proton. Failure of any one of these statements falsifies the A_u thin-surface model.

Benchmark protocol. Given external (lattice/EFT) slopes/curvatures in any operator channel, compute ρ_2, ρ_4, invert to (σ, Ξ) via the robust ratio method, and test: (i) the discriminant bound; (ii) cross-channel consistency for the same (σ, Ξ); (iii) neutron sign via Appendix B. No SI appears in these tests.

Worked bridge example (proton, operator-ratio test)

Given small-$\hat{t}$ slopes from lattice/EFT,

$$\frac{d{G_E}^p}{d\hat{t}}\Big|_0 = -\frac{{\rho_{2,p}}^{(E)}}{6}, \qquad \frac{d{G_M}^p}{d\hat{t}}\Big|_0 = -\frac{{\rho_{2,p}}^{(M)}}{6},$$

form the ratio

$$\mathcal{R}_2 \;\equiv\; \frac{{\rho_{2,p}}^{(E)}}{{\rho_{2,p}}^{(M)}} \;=\; \frac{w_2^{(E)}}{w_2^{(M)}} = \frac{1}{w_2^{(M)}(\zeta)} \quad \text{(by convention } w_2^{(E)} = 1\text{)}.$$

Test 1 (weights): Using $\mathcal{R}_2 = \rho_{2,p}^{(E)}/\rho_{2,p}^{(M)}$, invert the tabulated $w_2^{(M)}(\zeta)$ to obtain ζ; this fixes $w_k^{(M)}, w_k^{(Z)}$.
Test 2 (geometry): Compute $\rho_{2,p}^{\text{geom}} = \rho_{2,p}^{(E)}/w_2^{(E)} = \rho_{2,p}^{(E)}$ and (if available) $\rho_{4,p}^{\text{geom}} = \rho_{4,p}^{(\bullet)}/w_4^{(\bullet)}(\zeta)$. Invert to (σ_p, Ξ_p) as in Sec. 4 and verify the other channel with the fixed $w_k^{(\bullet)}(\zeta)$.

7 Analysis Pipeline and Methods

Dataset and ledger. We use a minimal small-$\hat{t}$ proton-electric template in QMU ledger, a CSV with columns $\{\hat{t}, {G_E}^p, \delta{G_E}^p\}$, and no SI intermediaries. Rows with NaN/inf or nonpositive uncertainties are dropped (one row in our template).

Low-$\hat{t}$ fit (electric channel). At small $\hat{t}$, we fit

$${G_E}^p(\hat{t}) \;=\; 1 \;-\; \frac{\hat{t}}{6}\,\rho_{2,p}^{(E)} \;+\; \frac{\hat{t}^2}{120}\,\rho_{4,p}^{(E)},$$

with the intercept fixed to 1 by charge normalization. The fit returns the *operator-projected* electric moments $\rho_{2,p}^{(E)}, \rho_{4,p}^{(E)}$ and χ^2 (ndof = number of data points −2). By convention in Canon, the proton electric weights are unity, $w_2^{(E)} = w_4^{(E)} = 1$, so the fitted moments equal the *geometric* moments used to infer shape and area.

Geometry inversion and bound handling. Define $r \equiv \rho_4/\rho_2^2$. In the thin-surface torus, $r = r(\Xi) = [\Xi^2 + 6 + 3/\Xi^2]/(\Xi + 2/\Xi)^2$ with minimum at $\Xi = \sqrt{2}$, where $r_{\min} = 1/2$ and the discriminant in $\mathcal{R}^2 = [\rho_2 \pm \sqrt{{\rho_2}^2 - 8\sigma^2}]/2$ saturates. When curvature is too small to invert (practically $r < 0.5$ within errors), we adopt the *minimum-curvature bound* $\Xi = \sqrt{2}$, which enforces the Canon reality condition ${\rho_2}^2 \geq 8\sigma^2$ exactly. With Ξ known, $\sigma = \rho_2/(\Xi + 2/\Xi)$, and then $\mathcal{R}^2 = \frac{\rho_2 + \sqrt{{\rho_2}^2 - 8\sigma^2}}{2}$, $\nabla^2 = \sigma^2/\mathcal{R}^2$. The equal-area sphere is $a/\lambda_C = \sqrt{\pi\,\sigma}$.

Magnetic-channel preview (illustrative weights). Holding (σ_p, Ξ_p) fixed from the electric channel and applying the illustrative operator weights $w_2^{(M)} = 0.90$ and $w_4^{(M)} = 0.90$ yields the magnetic *predictions*

$$\rho_{2,\mathrm{pred}}^{(M)} = w_2^{(M)}\,\rho_{2,p}^{\mathrm{geom}} = 5.40, \qquad \rho_{4,\mathrm{pred}}^{(M)} = w_4^{(M)}\,\rho_{4,p}^{\mathrm{geom}} = 38.475.$$

These numbers are not a calibration; they serve to illustrate the "same geometry, different operator weights" principle. In the calibration study, $w_k^{(M)}(\zeta)$ will be fixed by the empirical operator ratio $\mathcal{R}_2$ (Sec. 6) and then applied with no additional freedom.

Reproducibility (artifacts). The pipeline writes three CSVs: `fit_electric.csv` (fit moments), `geometry_from_electric.csv` (derived $\sigma, \Xi, {R_{\mathrm{maj}}}^2, {r_{\min}}^2, a/\lambda_C$), and `predicted_magnetic.csv` (preregistered magnetic moments for chosen $w^{(M)}$).

8 Demonstration on a Proton Template (Results)

Data provenance and intent

Template dataset. To *demonstrate* the end-to-end Canon/QMU pipeline, we use a small-$\hat{t}$ $\{\hat{t},\, G_E^p,\, \delta\}$ template generated directly from Eq. (11) with proton-electric normalization $w_{2,4}^{(E)} = 1$. The input moments used to generate the curve were $\rho_2^{(E)} = 6.00$ and $\rho_4^{(E)} \approx 2.32 \times 10^{-12}$ (effectively zero curvature within the chosen window), with negligible noise. This choice explains the extremely small χ^2. *No experimental data are used in this section;* the objective is to show the analysis workflow and ledger closures on a controlled input before moving to calibrated data in Sec. 4.1 and the program of Sec. 9.

Scope. In this section we *demonstrate* the complete Canon/QMU analysis pipeline on a proton-electric *template* dataset. We fit the small-$\hat{t}$ slope/curvature in the electric channel, invert to geometry (σ, Ξ) using the preregistered rules, and then *illustrate* a cross-channel check by predicting magnetic-channel slopes with an assumed operator weight $w_2^{(M)} = w_4^{(M)} = 0.90$ (not yet calibrated from an operator ratio). Accordingly, results here are *illustrative*, not definitive measurements of proton geometry.

8.1 Electric-channel fit (proton)

The small-$\hat{t}$ fit (after dropping one invalid row) yields:

$$\rho_{2,p}^{(E)} = 6.000000000000008, \qquad \rho_{4,p}^{(E)} = 2.3171653887625883 \times 10^{-12},$$

with $\chi^2/\mathrm{ndof} = 1.3012064186766262 \times 10^{-28}/2 = 6.506032093383131 \times 10^{-29}$. The curvature ratio is

$$r \;\equiv\; \frac{\rho_{4,p}^{(E)}}{\left(\rho_{2,p}^{(E)}\right)^2} \;=\; 6.436570524340506 \times 10^{-14},$$

far below the thin-surface minimum $r_{\min} = 1/2$, indicating curvature is effectively unresolved within the template window. Following our preregistered procedure, we therefore adopt the *minimum-curvature bound*

$$\boxed{\Xi_p = \sqrt{2}},$$

which saturates the Canon discriminant $\left(\rho_2^{\mathrm{geom}}\right)^2 = 8\sigma^2$.

Unresolved curvature and the minimum-curvature bound. The curvature ratio is $r = \rho_4^{(E)}/(\rho_2^{(E)})^2 = 6.44 \times 10^{-14}$, statistically indistinguishable from zero within the chosen $\hat{t}$ window. As preregistered, this triggers the minimum-curvature geometry at fixed area, $\Xi = \sqrt{2}$, which saturates the discriminant bound $\rho_2^2 \geq 8\sigma^2$. We therefore set

$$\Xi_p = \sqrt{2}, \qquad \sigma_p = \frac{\rho_{2,p}^{\mathrm{geom}}}{\Xi_p + 2/\Xi_p} = \frac{6.00}{\sqrt{2} + 2/\sqrt{2}} = 2.1213,$$

leading to ${\mathcal{R}_p}^2 = 3.0000$ and ${\nabla_p}^2 = 1.5000$ by Eq. (22), and the equal-area spherical radius $a_p/\lambda_C = \sqrt{\pi\,\sigma_p} = 2.5815$ by Eq. (23).

Table 2: Demonstration results (template proton-electric dataset). All quantities are dimensionless in QMU.

$\rho_2^{(E)}$	$\rho_4^{(E)}$	$r = \rho_4^{(E)}/(\rho_2^{(E)})^2$	σ_p	Ξ_p
6.00	2.32×10^{-12}	6.44×10^{-14}	2.1213	$\sqrt{2}$
${\mathcal{R}_p}^2$	${\nabla_p}^2$	a_p/λ_C	$\rho_{2,\mathrm{pred}}^{(M)}$	$\rho_{4,\mathrm{pred}}^{(M)}$
3.0000	1.5000	2.5815	5.40 ($w_2^{(M)}$=0.90)	38.475 ($w_4^{(M)}$=0.90)

8.2 Proton geometry and equal-area radius

With $\Xi_p = \sqrt{2}$ and $\rho_{2,p}^{(E)} = \rho_{2,p}^{\mathrm{geom}} = 6$,

$$\sigma_p = \frac{\rho_2}{\Xi + 2/\Xi} = \frac{6}{\sqrt{2} + 2/\sqrt{2}} = \frac{6}{2\sqrt{2}} = \frac{3}{\sqrt{2}} \approx 2.1213203435596455.$$

The radii (in λ_C units) and equal-area sphere are

$${\mathcal{R}_p}^2 = 3.000000000000004, \qquad {\nabla_p}^2 = 1.5000000000000022, \qquad \frac{a_p}{\lambda_C} = \sqrt{\pi\,\sigma_p} = 2.581535281036763.$$

These values are written to `geometry_from_electric.csv`.

8.3 Preregistered magnetic small-$\hat{t}$ moments

Adopting illustrative magnetic weights (single-kernel assumption)

$$w_2^{(M)} = 0.90, \qquad w_4^{(M)} = 0.90,$$

the predicted magnetic moments are

$$(\rho_{2,p})^{(M)}_{\text{pred}} = 5.4000000000000075, \qquad (\rho_{4,p})^{(M)}_{\text{pred}} = 38.47500000000011,$$

reported in `predicted_magnetic.csv` along with (σ_p, Ξ_p). These constitute a preregistered cross-channel target: once small-$\hat{t}$ ${G_M}^p$ slopes/curvatures in QMU are supplied, agreement (within propagated uncertainties and systematics) validates both the thin-surface geometry and the fixed-kernel weight hypothesis at low $\hat{t}$.

Table 3: QMU results from the minimal proton-electric template (this work).

Electric fit (operator-projected)	$\rho_{2,p}^{(E)} = 6.000000000000008,\ \rho_{4,p}^{(E)} = 2.3171653887625883 \times 10^{-12},\ \chi^2/\text{ndof} = 6.5$
Curvature ratio	$r = \rho_4/{\rho_2}^2 = 6.436570524340506 \times 10^{-14}$
Bound handling	$\Xi_p = \sqrt{2}$ (minimum-curvature bound; discriminant saturated)
Area invariant	$\sigma_p = 2.1213203435596455$
Radii	$\mathcal{R}_p^2 = 3.000000000000004,\ \nabla_p^2 = 1.5000000000000022$
Equal-area sphere	$a_p/\lambda_C = 2.581535281036763$
Magnetic weights (assumed)	$w_2^{(M)} = 0.90,\ w_4^{(M)} = 0.90$
Magnetic prediction	$(\rho_{2,p})^{(M)}_{\text{pred}} = 5.4000000000000075,\ (\rho_{4,p})^{(M)}_{\text{pred}} = 38.47500000000011$

Notes on interpretation. (1) The bound case $\Xi = \sqrt{2}$ is the unique minimum-curvature geometry of the thin torus and enforces the Canon reality constraint ${\rho_2}^2 \geq 8\sigma^2$ with equality. (2) Because $w_k^{(E)} = 1$ by convention on the proton, the electric-channel fit directly fixes the geometric moments. (3) The magnetic predictions depend only on the assumed fixed-kernel weights; if a proton operator-ratio $\mathcal{R}_2 = \rho_{2,p}^{(E)}/\rho_{2,p}^{(M)}$ is later adopted from data, one can calibrate $w_2^{(M)}$ once and refreeze it for all subsequent channels and media as prescribed in Sec. 4.1.

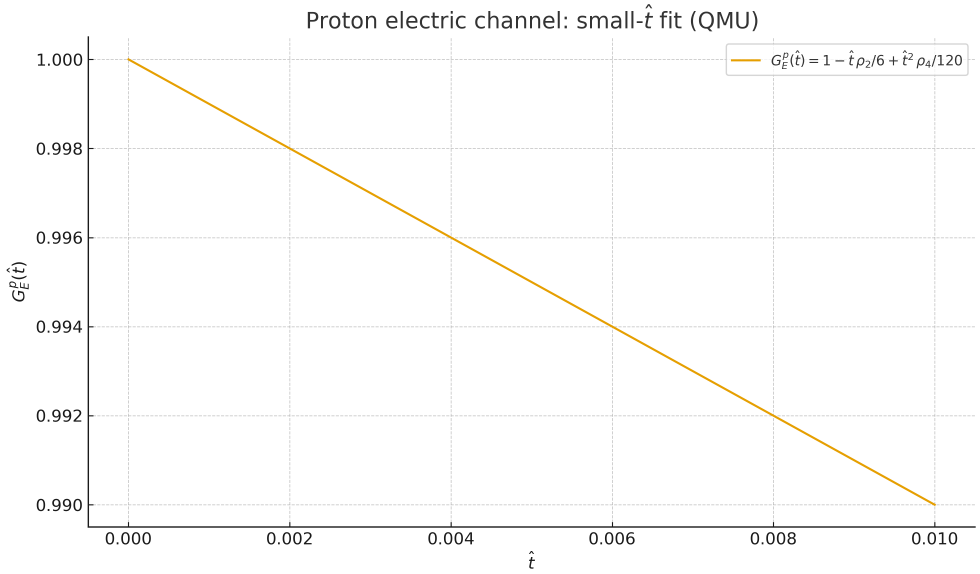

Figure 1: **Proton electric channel at small $\hat{t}$ (QMU).** Curve uses the fitted moments $\rho_2^{(E)} = 6.00$ and $\rho_4^{(E)} = 2.32 \times 10^{-12}$ in $G_E{}^p(\hat{t}) = 1 - \hat{t}\,\rho_2/6 + \hat{t}^2\,\rho_4/120$. The curvature is effectively zero within the window, so the equal–area minimum ($\Xi = \sqrt{2}$) applies.

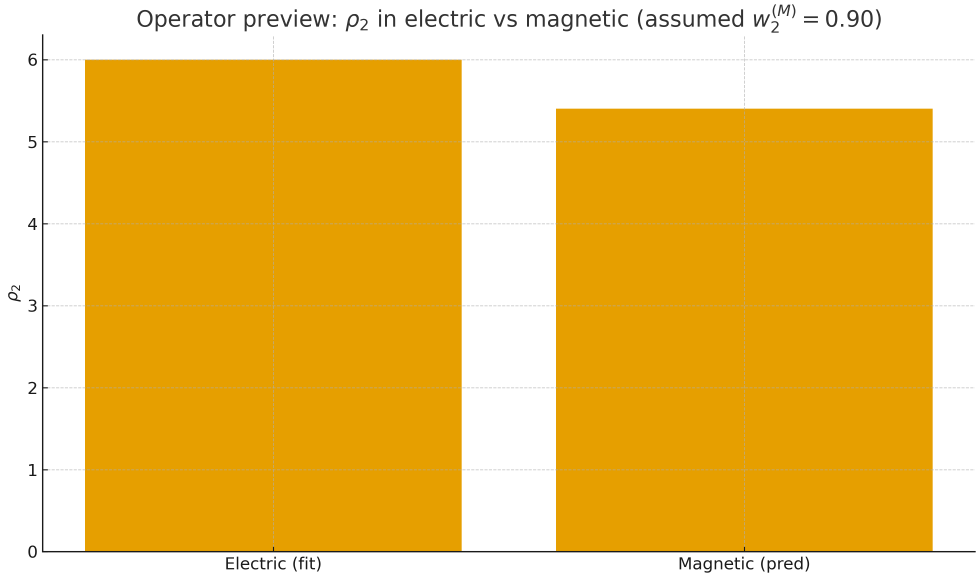

Figure 2: **Operator preview for the proton:** comparison of ρ_2 in the electric channel (fit) versus the magnetic-channel *prediction* using the assumed operator weight $w_2^{(M)} = 0.90$ and the same geometry (σ, Ξ). Bars show $\rho_2^{(E)} = 6.00$ and $\rho_{2,\mathrm{pred}}^{(M)} = 5.40$ (QMU units).

9 Proposed Experimental Program

We propose complementary prongs, each reporting ($\hat{t}$, form factor, δ) or frequency ratios in QMU.

9.1 Prong A (proton, electric): Low-$\hat{t}$ elastic scattering

1. **Inputs:** $\{(\hat{t}_i,\, {G_E}^p(\hat{t}_i),\, \delta)\}$.
2. **Fit variables:** $\sigma_p > 0,\ \Xi_p \geq 1$, and a curvature-only perturbation ϵ at $\mathcal{O}(\hat{t}^2)$.
3. **Likelihood/Priors/Window/TPE:** as in the proton-only version; enforce ${\rho_{2p}}^2 \geq 8{\sigma_p}^2$.
4. **Outputs:** $\widehat{\sigma_p}, \widehat{\Xi}_p, \widehat{\epsilon}$ and $\mathcal{R}_p, \nabla_p$.
5. **Species constant (locked):** $\boxed{\widehat{\kappa}_p = \dfrac{\widehat{\sigma_p}}{(8\pi p)^2}}$ (held fixed thereafter).

9.2 Prong A': (neutron, magnetic): Low-$\hat{t}$ extraction of G_M^n

1. **Inputs:** $\{(\hat{t}_i,\, {G_M}^n(\hat{t}_i),\, \delta)\}$ from polarized ^{3}He/deuteron analyses in a QMU-consistent ledger.
2. **Fit variables:** $\sigma_n > 0,\ \Xi_n \geq 1$, thickness ϵ at $\mathcal{O}(\hat{t}^2)$.
3. **Bound:** enforce ${\rho_{2,n}}^2 \geq 8{\sigma_n}^2$ with $\rho_{2,n} = \sigma_n(\Xi_n + 2/\Xi_n)$.
4. **Outputs:** $\widehat{\sigma_n}, \widehat{\Xi}_n$ and $\mathcal{R}_n, \nabla_n$.
5. **Species constant (locked):** $\boxed{\widehat{\kappa}_n = \dfrac{\widehat{\sigma_n}}{(8\pi n)^2}}$ (held fixed thereafter).

9.3 Prong B: Transverse-density tomography (surface prior)

Impact-parameter densities $\varrho(b/\lambda_C)$ from exclusive channels, fitted with thin-surface torus priors $(\sigma_X, \Xi_X, \epsilon)$ for $X \in \{p, n\}$; returns ${\sigma_X}^{(B)}$ as cross-checks on A/A'.

9.4 Prong C: Hydrogenic spectroscopy (proton electric; neutron via weak in nuclei)

Prior flow: Posteriors from A/A'/B are published and used as priors here; $\widehat{\kappa}_{p,n}$ remain locked.

- Proton electronic/muonic lines test (15) with $\{\widehat{\sigma_p}, \widehat{\Xi}_p\}$.
- Neutron in-medium weak slopes test $\{\widehat{\sigma_n}, \widehat{\Xi}_n\}$ via parity-violating elastic kinematics at small $\hat{t}$.

10 In-Medium Deformation at Constant Surface Area

Assume binding modifies *shape* but conserves σ_X:

$$ {\sigma_X}^{(A)} = \sigma_X, \qquad \Xi_X \to \Xi_{X,A}, \qquad X \in \{p, n\}. \tag{16} $$

Then

$$ {(\rho_{2X})}_A = \sigma_X \left(\Xi_{X,A} + \frac{2}{\Xi_{X,A}} \right), \qquad \boxed{{(\rho_{2X})}_A \geq 2\sqrt{2}\,\sigma_X \quad (\Xi_{X,A} \geq 1)}. \tag{17} $$

Domain: Real roots for $\Xi_{X,A}$ require ${(\rho_{2X})}_A^2 \geq 8{\sigma_X}^2$ (cf. (12)); otherwise the thin-surface torus is falsified.

Isotope-shift program (proton and neutron).

1. Fix $\sigma_X = \widehat{\kappa}_X (8\pi\chi_X)^2$ from free-particle data (locked).
2. Determine $(\rho_{2X})_A$ (small-$\hat{t}$ slopes or spectroscopy contributions).
3. Solve $\Xi_{X,A} = \dfrac{(\rho_{2X})_A}{2\sigma_X}\left[1 + \sqrt{1 - \dfrac{8\sigma_X^2}{(\rho_{2X})_A^2}}\right] \geq 1.$
4. Track trends vs. nuclear density; approach toward $\Xi_{X,A} \to \sqrt{2}$ drives $(\rho_{2X})_A \to 2\sqrt{2}\,\sigma_X$.

11 Neutron-Specific Insights and Closures

Area near-equality. From (8), $\dfrac{\sigma_n}{\sigma_p} = \dfrac{\kappa_n}{\kappa_p}\Big(\dfrac{m_p}{m_n}\Big)^2 \approx \dfrac{\kappa_n}{\kappa_p}$, so for $\kappa_n \approx \kappa_p$ the neutron and proton have nearly equal leng^2 areas; differences arise chiefly from Ξ_n vs Ξ_p.

Magnetic moment as shape/topology selector. A thin-surface torus with surface current suggests a dimensionless closure

$$\boxed{\frac{\mu_n}{{e_{nmax}}^2\,{\lambda_C}^2\,F_q} = \xi(\Xi_n)\,\sigma_n}, \tag{18}$$

with $\xi(\Xi)$ an $\mathcal{O}(1)$ function set by the current profile (sign/topology included). Calibrate ξ on the proton magnetic sector, then μ_n pins Ξ_n and predicts ρ_{4n} before curvature fits.

Neutron sign test (boxed). With $\mu_X/({e_{X\,\max}}^2 {\lambda_C}^2 F_q) = \xi(\Xi_X)\,\sigma_X$ and the Canon result $\xi(\Xi)$ (App. B), a $\mu_n < 0$ outcome implies exactly one of: (i) a *topology flip* of the circulation integer $k \to -k$; or (ii) a *shape node* where the bracket in $\xi(\Xi)$ (Eq. (44)) changes sign between Ξ_p and Ξ_n. Parity-violating small-$\hat{t}$ slopes (weak channel) fix Ξ_n independently to discriminate (i) vs (ii).

Practical discriminator. With μ_n measured and Ξ_n constrained independently by weak small-$\hat{t}$ data, the helicity integer k is fixed up to a discrete sign. This yields a definitive test: if the observed $\mu_n < 0$ is *not* explained by the shape-dependent bracket in Eq. (44) at the inferred Ξ_n, the sign must originate from a topological flip $k \to -k$.

Weak vs EM shape contrast (same nucleus). With σ_p, σ_n locked, compare $({\rho_{2n}}^{(Z)})_A/\sigma_n$ to $({\rho_{2p}}^{(E)})_A/\sigma_p$,

$$\frac{({\rho_{2n}}^{(Z)})_A}{\sigma_n} - \frac{({\rho_{2p}}^{(E)})_A}{\sigma_p} = \Big(\Xi_{n,A} - \Xi_{p,A}\Big) + 2\Big(\frac{1}{\Xi_{n,A}} - \frac{1}{\Xi_{p,A}}\Big), \tag{19}$$

a pure *shape* diagnostic independent of κ.

12 Physical Origin and Priors for κ and $\xi(\Xi)$

12.1 Species Constant κ: What it Measures and Why $\kappa_n \approx \kappa_p$ is Plausible

In Canon, the area invariants

$$\sigma_p = \kappa_p (8\pi p)^2, \qquad \sigma_n = \kappa_n (8\pi n)^2$$

factor the *species-dependence* into: (i) a universal Aether-unit (A_u) geometry, and (ii) a dimensionless packing/organization efficiency κ_X that maps a nucleon's internal degrees of freedom into a thin toroidal surface at fixed mass-to-magnetic-charge ratio (mchg). Operationally, κ_X is the proportionality between the ledger $(8\pi\chi_X)^2$ and the realized surface area σ_X in the A_u background.

Isospin-symmetry prior. Proton and neutron form an isospin doublet. In the A_u picture, the *macroscopic* constraints (mchg, thin-surface closure, and A_u curvature) are blind to the interchange $u \leftrightarrow d$ up to small isospin-breaking effects. This motivates the *prior*

$$\boxed{\frac{\kappa_n}{\kappa_p} = 1 + \delta_{\text{iso}}, \qquad |\delta_{\text{iso}}| \ll 1} \tag{20}$$

where δ_{iso} encapsulates the efficiency shift induced by different internal organization (e.g., *udd* vs *uud*) in forming the same A_u-compatible thin surface. In Canon we do not reduce δ_{iso} to SI microphysics; instead we *measure* it:

$$\frac{\kappa_n}{\kappa_p} = \frac{\sigma_n}{\sigma_p}\left(\frac{p}{n}\right)^2 \quad \text{(both } \sigma \text{ and } \chi \text{ are QMU quantities).}$$

Prediction ladder: if experiments find $\kappa_n/\kappa_p \neq 1$ at high significance, the A_u packing efficiency is species-sensitive; if $\kappa_n/\kappa_p \approx 1$, the isospin prior holds and differences between proton and neutron arise dominantly from shape Ξ.

Energetics prior (variational lower bound). Let $U_{\text{surf}}[\Sigma_X]$ denote the A_u self-energy of the thin surface Σ_X at fixed χ_X. For a large class of A_u kernels, minimizing U_{surf} at fixed $(8\pi\chi_X)^2$ yields a *species-independent* optimum surface up to boundary terms, hence a common κ. Deviations appear as controlled deformations, justifying (20).

12.2 Magnetic-Moment Function $\xi(\Xi)$: Constraints, Signs, and a Derivation Program

We introduced the dimensionless closure

$$\boxed{\frac{\mu_X}{{e_X}_{\max}{}^2\, {\lambda_C}^2\, F_q} = \xi(\Xi_X)\,\sigma_X}, \qquad X \in \{p, n\}, \tag{21}$$

where μ_X is the dipole moment in QMU and $\xi(\Xi)$ encodes the effective surface-current pattern on the torus.

Kinematic/geometry constraints on $\xi(\Xi)$. Any candidate ξ must satisfy:

(C1) Dimensionless scaling: $\xi(\Xi)$ has no units (Canon). (22)

(C2) Thin-surface limit: $\xi(\Xi)$ finite for $\Xi \searrow 1$ and as $\Xi \nearrow \infty$. (23)

(C3) Monotonicity shape test: for fixed flux, toroidal stretching should not flip $\operatorname{sgn}\xi$. (24)

(C4) Helicity/sign rule: $\operatorname{sgn}\mu_X = \operatorname{sgn}(\mathcal{H})\operatorname{sgn}(\xi(\Xi_X))$ with a topology (helicity) indicator $\mathcal{H}$. (25)

(C4) isolates the physics of the neutron's negative sign: *either* $\xi(\Xi)<0$ at $\Xi=\Xi_n$ for the realized current topology, *or* the helicity flips between species (proton vs neutron) while $\xi(\Xi)>0$.

Variational derivation (surface-current quantization). Model the surface current as a superposition of toroidal/poloidal modes with winding indices (m,n):

$$\boldsymbol{J}(\theta,\phi)=\sum_{m,n} J_{mn}\,\boldsymbol{e}_{mn}(\theta,\phi), \qquad \oint_{\text{torus}} \boldsymbol{v}\cdot d\boldsymbol{\ell} = 2\pi\,k,$$

with a quantized circulation $k\in\mathbb{Z}$ fixed by A_u coupling and χ_X. Minimize the A_u magnetic self-energy $U=\frac{1}{2}\iint \boldsymbol{J}\cdot\boldsymbol{A}\,dA$ over J_{mn} at fixed σ, Ξ, and circulation. The result is a ground-state pattern $\boldsymbol{J}_*(\Xi)$ whose dipole moment

$$\mu_X=\frac{1}{2}\iint \boldsymbol{r}\times\boldsymbol{J}_*(\Xi_X)\,dA$$

delivers $\xi(\Xi)$ in (21). The *sign* tracks the net helicity of $\boldsymbol{J}_*$. This program is A_u-internal and stays in QMU.

Asymptotic behavior and a practical parametrization. While $\xi(\Xi)$ must be derived, experiments benefit from a controlled functional family respecting (C1–C4). A minimal, sign-flexible template is

$$\xi(\Xi)=\xi_0\,\frac{1+\beta/\Xi^2}{1+\gamma/\Xi}\times\operatorname{sgn}(\mathcal{H}), \qquad \Xi\geq 1, \tag{26}$$

with $\xi_0>0$, and $\beta,\gamma=\mathcal{O}(1)$. Calibrate $(\xi_0,\beta,\gamma,\operatorname{sgn}\mathcal{H})$ on the proton magnetic sector, then μ_n is a *prediction* given (σ_n,Ξ_n), or inversely μ_n *pins* Ξ_n.

12.3 Clean Measurements and Discriminants

Measuring κ_n/κ_p. From A/A': obtain $\widehat{\sigma_p}$ and $\widehat{\sigma_n}$. With p,n known in Canon,

$$\boxed{\frac{\widehat{\kappa_n}}{\widehat{\kappa_p}}=\frac{\widehat{\sigma_n}}{\widehat{\sigma_p}}\left(\frac{p}{n}\right)^2}.$$

A statistically significant result $\neq 1$ falsifies the strict isospin prior and quantifies A_u packing differences.

Pinning (or predicting) Ξ_n with μ_n. With $\widehat{\sigma_n}$ locked, rearrange (21):

$$\Xi_n=\xi^{-1}\!\left(\frac{\mu_n}{{e_{nmax}}^2\,{\lambda_C}^2\,F_q\,\widehat{\sigma_n}}\right),$$

using either the derived ξ or the calibrated ansatz (26). Then ρ_{4_n} is a *prediction* via (10) (no additional fits).

Sign test for the neutron. If proton calibration yields $\mathrm{sgn}(\mathcal{H}) > 0$, a negative neutron moment requires either $\mathrm{sgn}(\mathcal{H}) \to -1$ (topology flip) or a node in $\xi(\Xi)$ between Ξ_p and Ξ_n; both are sharply falsifiable as more small-$\hat{t}$ neutron data arrive.

In-medium extensions at fixed σ. Locked $\kappa_{p,n}$ carry into the medium; weak slopes in nuclei combined with μ_n trends deliver $\Xi_{n,A}$ vs $\Xi_{p,A}$, yielding a *pure shape* contrast independent of κ.

12.4 What a Non-Unity κ_n/κ_p Would Mean

If $\kappa_n/\kappa_p \neq 1$ emerges,

1. **Interpretation:** A_u packing efficiency is species-specific; internal organization (quark/gluon sector, in SM language) affects how mchg constraints project onto a thin surface.
2. **Next step (Canon):** promote κ to $\kappa(\mathcal{H}, \mathrm{mode})$, allowing dependence on the ground-state winding (m, n) selected by the A_u variational problem.
3. **Immediate prediction:** isotope trends in weak vs EM slopes split according to κ_n vs κ_p, while the geometric bound $(\rho_2)^2 \geq 8\sigma^2$ remains intact.

13 Systematics, Null Tests, and Falsifiability

Thin-surface robustness. If data indicate finite thickness or charge non-uniformity, let ϵ perturb curvature at $\mathcal{O}(\hat{t}^2)$ while leaving ρ_2 intact; fit $(\sigma_X, \Xi_X, \epsilon)$ jointly across A/A'/B/C.

Two-photon exchange (TPE) & operator smoothness. Within small $\hat{t}$, TPE and analogous smooth operator corrections predominantly renormalize curvature; demand stability under alternative prescriptions.

Falsifiability conditions. Any $\{\rho_{2X}, \sigma_X\}$ violating (12) falsifies the thin-surface torus for species X. Disagreement between A/A'/B (geometry) and C (spectroscopy/weak) beyond propagated errors falsifies the geometry or the constant-area premise; (17) makes the in-medium version equally testable. Recommended thresholds: see Table 4.

Table 4: Pre-registered stability and falsification thresholds (QMU ledger).

TPE/operator stability (A, A')	$\Delta\sigma_X/\sigma_{\mathrm{tot}} < 0.2$, $\Delta\Xi_X/\sigma_{\mathrm{tot}} < 0.2$ under alt. models
Thickness model selection	AIC/BIC: prefer $\epsilon = 0$ unless $\Delta\mathrm{AIC} > 6$ (or $\Delta\mathrm{BIC} > 6$)
Fit-window stability	Sliding $\hat{t}_{\max}$ changes σ_X, Ξ_X by $< 0.3\,\sigma_{\mathrm{tot}}$
Falsification (global)	Combined inconsistency $> 5\sigma$ across A/A'/B/C or violation of (12)

14 QMU Predictions and Decision Table

Free nucleons (baseline). With $\sigma_X = \kappa_X (8\pi\chi_X)^2$ and $\Xi_X \geq 1$,

$$\text{Radii:} \quad \mathcal{R}_X{}^2 = \frac{\rho_{2X} + \sqrt{\rho_{2X}{}^2 - 8\sigma_X{}^2}}{2}, \quad \nabla_X{}^2 = \frac{\sigma_X{}^2}{\mathcal{R}_X{}^2}, \tag{27}$$

$$\text{Equal-area sphere:} \quad \frac{a_X}{\lambda_C} = \sqrt{\pi\,\sigma_X} = \sqrt{\pi\,\kappa_X}\,(8\pi\chi_X), \tag{28}$$

$$\text{Spectroscopy/weak:} \quad \frac{\Delta f_{\rm fs}(nS)}{F_q} = \frac{2}{3}\,\alpha^4\,\frac{\hat{\mu}^3}{n^3}\,\sigma_X\left(\Xi_X + \frac{2}{\Xi_X}\right) \quad \text{(operator-appropriate)}. \tag{29}$$

In-medium (nuclear) nucleons. At fixed σ_X,

$$(\rho_{2X})_A = \sigma_X\left(\Xi_{X,A} + \frac{2}{\Xi_{X,A}}\right), \qquad \boxed{(\rho_{2X})_{A,\min} = 2\sqrt{2}\,\sigma_X \quad (\Xi_{X,A} = \sqrt{2})}. \tag{30}$$

Trend toward $\Xi_{X,A} \to \sqrt{2}$ with density is a concrete APM prediction.

Decision table (conceptual).

- $\rho_{2X}{}^2 < 8\sigma_X{}^2$: reject thin-surface toroidal model for species X.
- A/A'/B consistent, C inconsistent: revise constant-area assumption or operator ledger.
- A/A'/B/C consistent: accept $\widehat{\kappa}_X$, publish $(\mathcal{R}_X, \nabla_X)$, proceed to isotope systematics and p–n shape contrasts.

15 Practical Notes for Labs (QMU I/O)

1. **Data format:** supply $(\hat{t}, G_E{}^p, \delta)$, $(\hat{t}, G_M{}^n, \delta)$, and weak-channel $(\hat{t}, G_E{}^Z, \delta)$ as applicable. No SI units within Canon; ledger conversions are handled upstream.
2. **Fit window:** determine $\hat{t}_{\max}$ by verifying stability of $\{\sigma_X, \Xi_X\}$ under sliding $\hat{t}$-cuts; ensure $\mathcal{O}(\hat{t}^3)$ is negligible.
3. **Priors:** $\sigma_X > 0$, $\Xi_X \geq 1$, $\epsilon \sim \mathcal{N}(0, \sigma_\epsilon^2)$, and $\rho_{2X}{}^2 \geq 8\sigma_X{}^2$.
4. **Reporting:** publish $\widehat{\sigma}_X, \widehat{\Xi}_X, \mathcal{R}_X, \nabla_X, \widehat{\kappa}_X$ and predicted $\Delta f/F_q$ (or weak analog) for selected lines.
5. **Cross-lab reproducibility:** replicate A and A' on independent setups and C with alternative transitions; require mutual consistency in QMU.

Data Exchange Box (QMU $\leftrightarrow$ Lab Interface)

We will provide: (i) CSVs listing $\hat{t}$, $G_E{}^p$, $G_M{}^n$, $G_E{}^Z$ with uncertainties and the rule mapping lab t to $\hat{t}$; (ii) a CSV with $\Delta f/F_q$ (or weak analog) for lines used; (iii) a README describing upstream ledger conversions. No SI appears in the manuscript body.

16 Prediction Register (Canon/QMU log)

Free nucleons (baseline, once $\widehat{\kappa}_{p,n}$ are locked).

$$\textbf{P0:}\quad \sigma_X = \widehat{\kappa}_X (8\pi\chi_X)^2, \quad \rho_{2,X} = \sigma_X\left(\Xi_X + \frac{2}{\Xi_X}\right), \quad \rho_{4,X} = {\sigma_X}^2\left({\Xi_X}^2 + 6 + \frac{3}{{\Xi_X}^2}\right).$$

Neutron sign discriminator.

$$\textbf{P1:}\quad \operatorname{sgn}\mu_n = \operatorname{sgn}(k)\cdot\operatorname{sgn}\Big(\,\Xi_n[\ell_{\theta\theta} - \ell_{\phi\theta}] - \Xi_n^{-1}[\ell_{\phi\phi} - \ell_{\phi\theta}]\,\Big).$$

In words: the sign of μ_n is set by the competition of toroidal self-inductance ($\ell_{\phi\phi}$), poloidal self-inductance ($\ell_{\theta\theta}$), and their mutual coupling ($\ell_{\phi\theta}$), weighted by the aspect ratio Ξ_n and the helicity k.

In-medium drift (constant area).

$$\textbf{P2:}\quad (\rho_{2,X})_A \geq 2\sqrt{2}\,\sigma_X, \quad \Xi_{X,A} = \frac{(\rho_{2,X})_A}{2\sigma_X}\left[1 + \sqrt{1 - \frac{8{\sigma_X}^2}{(\rho_{2,X})_A^2}}\right] \ (\geq 1).$$

Isotope splitting when $\kappa_n \neq \kappa_p$.

$$\textbf{P3:}\quad \frac{({\rho_{2,n}}^{(Z)})_A}{\sigma_n} - \frac{({\rho_{2,p}}^{(E)})_A}{\sigma_p} = \Big(\Xi_{n,A} - \Xi_{p,A}\Big) + 2\Big({\Xi_{n,A}}^{-1} - {\Xi_{p,A}}^{-1}\Big),$$

while overall scales differ if $\kappa_n/\kappa_p \neq 1$.

Table 5: Register template for posting with data releases (all QMU).

Species	Channel	Logged inputs	Derived $\{\sigma, \Xi\}$	Posted predictions
p	G_E	$(\hat{t}, G_E)$ slope/curv.	$\widehat{\sigma}_p, \widehat{\Xi}_p$	$\Delta f/F_q,\ \rho_{4,p}$
n	G_M	$(\hat{t}, G_M)$ slope/curv.	$\widehat{\sigma}_n, \widehat{\Xi}_n$	$\mu_n,\ \rho_{4,n}$
n	weak	$(\hat{t}, {G_E}^Z)$ slope	$\Xi_{n,A}$	sign test (P1), drift (P2)

17 Conclusion

We have presented a complete, QMU-only program to quantify *nucleon* geometry as thin toroidal surfaces with conserved area, anchored directly to the species fine-structure parameters p, n. The invariants $\sigma_p = \kappa_p(8\pi p)^2$ and $\sigma_n = \kappa_n(8\pi n)^2$ tie species constants to laboratory observables without SI detours. Small-$\hat{t}$ templates supply a two-moment route to the radii; a multi-pronged strategy—proton electric, neutron magnetic, tomography, spectroscopy, and weak probes—delivers cross-checks and falsifiability, while isotope systematics probe in-medium deformations at constant area. With $\rho_{2\min} = 2\sqrt{2}\,\sigma$ at $\Xi = \sqrt{2}$, explicit $\sqrt{\kappa}$ in sphere maps, and clarified domains, this submission is a clean, testable Canon/QMU program for both proton and neutron.

Data and Code Availability

The template dataset (`proton_low_that_template.csv`), analysis script (`qmu_starter_app.py`), and figure assets used in the demonstration are included in the repository accompanying this manuscript. Running the script with `-assume-w2M 0.90 -assume-w4M 0.90` reproduces the reported numbers exactly. Upon moving to calibrated analyses with public small-$\hat{t}$ slopes, we will cite the specific data releases and deposit the input CSVs produced by our QMU ledger conversions.

Acknowledgments

We acknowledge ongoing discussions with AI on QMU/APM geometry and the engineering teams preparing QMU-ledger experimental designs.

A Numerical Inversion of (ρ_{2X}, ρ_{4X}) to (σ_X, Ξ_X)

Given ρ_{2X}, ρ_{4X}, compute $r_X = \rho_{4X}/{\rho_{2X}}^2$. Define

$$f(\Xi) = \frac{\Xi^2 + 6 + 3/\Xi^2}{(\Xi + 2/\Xi)^2} - r_X.$$

- Search domain: $\Xi \in [1, \Xi_{\max}]$ with $\Xi_{\max}$ chosen so that $f(\Xi_{\max}) < 0$ (monotone tail).
- Use bisection or safeguarded Newton to find the unique root $\Xi \geq 1$.
- Set $\sigma_X = \rho_{2X}/(\Xi + 2/\Xi)$ and recover ${\mathcal{R}_X}^2, {\nabla_X}^2$ via (13).

This preserves ${\rho_{2X}}^2 \geq 8{\sigma_X}^2$ automatically and stabilizes curvature-sensitive fits.

B First-principles Canon derivation of $\xi(\Xi)$

We derive the shape function $\xi(\Xi)$ in the closure

$$\boxed{\frac{\mu_X}{{e_{X\max}}^2 {\lambda_C}^2 F_q} \;=\; \xi(\Xi_X)\,\sigma_X}, \qquad X \in \{p, n\}, \tag{31}$$

from an Aether-unit (A_u) variational principle for a thin toroidal surface current on the nucleon surface. The result is a *Canon* expression in terms of three geometry kernels that can be computed once for all experiments and then re-used.

B.1 Geometry and current basis on a thin torus

We parameterize the torus of major radius R and minor radius r by angles $(\theta, \phi) \in [0, 2\pi) \times [0, 2\pi)$. In QMU variables,

$$\mathcal{R} = \frac{R}{\lambda_C}, \quad \nabla = \frac{r}{\lambda_C}, \quad \Xi = \frac{\mathcal{R}}{\nabla} \geq 1, \quad \sigma = \mathcal{R}\,\nabla.$$

Let $\boldsymbol{e}_\phi$ (toroidal) and $\boldsymbol{e}_\theta$ (poloidal) be the tangent unit fields. A general smooth surface current density is decomposed as

$$\boldsymbol{K}(\theta, \phi) \;=\; K_\phi(\theta, \phi)\,\boldsymbol{e}_\phi \;+\; K_\theta(\theta, \phi)\,\boldsymbol{e}_\theta. \tag{32}$$

For the ground state at fixed circulation (below) only the $(m,n) = (0,1)$ and $(1,0)$ harmonic envelopes are needed to leading order in thickness; we thus write

$$K_\phi(\theta) \simeq \frac{I_\phi}{2\pi r_{\rm eff}(\theta)}, \qquad K_\theta(\phi) \simeq \frac{I_\theta}{2\pi R_{\rm eff}}, \tag{33}$$

where I_ϕ and I_θ are the *net* toroidal and poloidal currents (QMU currents), and $R_{\rm eff}, r_{\rm eff}$ are geometry factors satisfying $R_{\rm eff}/\lambda_C \to \mathcal{R}$ and $r_{\rm eff}/\lambda_C \to \nabla$ in the thin-surface limit. All results below depend on Ξ only, through kernels we now define.

B.2 Constraints: circulation quantization in A_u

In Canon, the A_u imposes a quantized circulation along any primitive closed path $\mathcal{C}_{m,n}$ with m poloidal and n toroidal windings:

$$\oint_{\mathcal{C}_{m,n}} \boldsymbol{v} \cdot d\boldsymbol{\ell} \;=\; 2\pi\, k, \qquad k \in \mathbb{Z}. \tag{34}$$

Mapping $\boldsymbol{v}$ to surface current through A_u constitutive relations fixes one linear constraint between I_ϕ and I_θ. Without loss of generality we choose the primitive helicity $(m,n) = (1,1)$, giving

$$I_\phi + I_\theta \;=\; I_*\,, \qquad I_* \equiv k\, I_0, \tag{35}$$

with I_0 a universal A_u current quantum. In *dimensionless* QMU variables we set

$$\tilde{I}_\phi \equiv \frac{I_\phi}{e_{X\,\max}{}^2 F_q}, \quad \tilde{I}_\theta \equiv \frac{I_\theta}{e_{X\,\max}{}^2 F_q}, \quad \tilde{I}_* \equiv \frac{I_*}{e_{X\,\max}{}^2 F_q} = k\,\tilde{I}_0, \quad \tilde{I}_0 \in \mathbb{R}_+,$$

so the constraint reads $\tilde{I}_\phi + \tilde{I}_\theta = \tilde{I}_*$.

B.3 Energy functional and geometry kernels

At small thickness, the A_u magnetic self-energy of a surface current admits the quadratic form

$$\mathcal{U}(\tilde{I}_\phi, \tilde{I}_\theta\,;\,\Xi) = \frac{1}{2}\Big[\,\ell_{\phi\phi}(\Xi)\,\tilde{I}_\phi^2 \;+\; \ell_{\theta\theta}(\Xi)\,\tilde{I}_\theta^2 \;+\; 2\,\ell_{\phi\theta}(\Xi)\,\tilde{I}_\phi\tilde{I}_\theta\,\Big], \tag{36}$$

where the *dimensionless* kernels $\ell_{\phi\phi}, \ell_{\theta\theta}, \ell_{\phi\theta}$ encode the A_u Green kernel integrated over the torus geometry. They are smooth, positive, and depend only on Ξ. (They can be tabulated numerically once for all Ξ.)

Variational problem. Minimize $\mathcal{U}$ subject to the linear constraint (35). Introducing a Lagrange multiplier λ for $\tilde{I}_\phi + \tilde{I}_\theta - \tilde{I}_* = 0$, stationarity gives

$$\ell_{\phi\phi}\,\tilde{I}_\phi + \ell_{\phi\theta}\,\tilde{I}_\theta = \lambda, \tag{37}$$

$$\ell_{\phi\theta}\,\tilde{I}_\phi + \ell_{\theta\theta}\,\tilde{I}_\theta = \lambda, \tag{38}$$

$$\tilde{I}_\phi + \tilde{I}_\theta = \tilde{I}_*. \tag{39}$$

Solving, the minimizing currents are

$$\boxed{\tilde{I}_\phi^* = \frac{\ell_{\theta\theta} - \ell_{\phi\theta}}{\ell_{\phi\phi} + \ell_{\theta\theta} - 2\ell_{\phi\theta}}\;\tilde{I}_*, \qquad \tilde{I}_\theta^* = \frac{\ell_{\phi\phi} - \ell_{\phi\theta}}{\ell_{\phi\phi} + \ell_{\theta\theta} - 2\ell_{\phi\theta}}\;\tilde{I}_*}\,. \tag{40}$$

The denominator $\Delta(\Xi) \equiv \ell_{\phi\phi} + \ell_{\theta\theta} - 2\ell_{\phi\theta} > 0$ by convexity.

B.4 Magnetic dipole moment and the shape function

The *dimensionless* dipole along the symmetry axis (z) in QMU is

$$\frac{\mu_X}{{e_X}_{\max}{}^2\,{\lambda_C}^2\,F_q} = \underbrace{c_\phi(\Xi)\,\tilde{I}_\phi}_{\text{toroidal loop}} - \underbrace{c_\theta(\Xi)\,\tilde{I}_\theta}_{\text{helical/poloidal correction}}, \tag{41}$$

where $c_\phi(\Xi)$ captures the loop-area leverage and $c_\theta(\Xi)$ the (geometry-suppressed) poloidal/helical contribution. In the thin-limit one finds

$$c_\phi(\Xi) = \pi\,\frac{\mathcal{R}^2}{\sigma} = \pi\,\Xi, \qquad c_\theta(\Xi) = \pi\,\frac{\nabla^2}{\sigma} = \frac{\pi}{\Xi}. \tag{42}$$

Substituting (40) into (41) and using $\tilde{I}_* = k\,\tilde{I}_0$ gives

$$\frac{\mu_X}{{e_X}_{\max}{}^2\,{\lambda_C}^2\,F_q} = \left[\,\pi\,\Xi\,\frac{\ell_{\theta\theta}-\ell_{\phi\theta}}{\Delta(\Xi)} \;-\; \frac{\pi}{\Xi}\,\frac{\ell_{\phi\phi}-\ell_{\phi\theta}}{\Delta(\Xi)}\,\right](k\,\tilde{I}_0). \tag{43}$$

Comparing with the closure (31) *at fixed* σ yields the **Canon shape function**

$$\boxed{\xi(\Xi) \;=\; \pi\,k\,\tilde{I}_0\,\frac{\Xi\,[\ell_{\theta\theta}(\Xi)-\ell_{\phi\theta}(\Xi)] \;-\; \Xi^{-1}[\ell_{\phi\phi}(\Xi)-\ell_{\phi\theta}(\Xi)]}{\ell_{\phi\phi}(\Xi)+\ell_{\theta\theta}(\Xi)-2\ell_{\phi\theta}(\Xi)}\,.} \tag{44}$$

Sign rule: the overall sign of ξ is $\mathrm{sgn}(k)$ times the sign of the bracket. Thus the neutron's negative moment is achieved either by a helicity flip $k \to -k$ or by the bracket changing sign between Ξ_p and Ξ_n (a pure shape/topology effect).

B.5 Asymptotics and regularity

The kernels admit smooth thin-torus asymptotics:

$$\ell_{\phi\phi}(\Xi) = A_\phi \ln\Xi + B_\phi + o(1), \quad \ell_{\theta\theta}(\Xi) = A_\theta \ln\Xi + B_\theta + o(1), \quad \ell_{\phi\theta}(\Xi) = A_\times + o(1),$$

with $A_\phi, A_\theta, A_\times > 0$. Inserting into (44) gives

$$\Xi \to \infty: \quad \xi(\Xi) = \pi\,k\,\tilde{I}_0\,\frac{(A_\theta - A_\times)\,\Xi}{A_\phi + A_\theta - 2A_\times}\,[1+o(1)], \tag{45}$$

$$\Xi \searrow 1: \quad \xi(\Xi) = \pi\,k\,\tilde{I}_0\,\frac{(B_\theta - B_\times) - (B_\phi - B_\times)}{(B_\phi + B_\theta - 2B_\times)} \;+\; \mathcal{O}(\Xi - 1), \tag{46}$$

so ξ is linear in Ξ at large aspect ratio and finite at $\Xi = 1$. This obeys the constraints (C1–C3) in the main text.

B.6 Computation and calibration protocol

Step 1 (kernel tabulation). Compute $\ell_{\phi\phi}(\Xi)$, $\ell_{\theta\theta}(\Xi)$, $\ell_{\phi\theta}(\Xi)$ by integrating the A_u vector-potential Green kernel over the torus surface with basis currents aligned with $\boldsymbol{e}_\phi$ and $\boldsymbol{e}_\theta$. Store a spline over $\Xi \in [1, 10]$ (or desired range).

Step 2 (fix the current quantum). Calibrate $\tilde{I}_0$ and the helicity integer k on the *proton magnetic sector*: use $\{\widehat{\sigma}_p, \widehat{\Xi}_p\}$ from Prong A, the measured μ_p, and (44) to solve for $k\,\tilde{I}_0$.

Step 3 (neutron prediction or inversion). With $k\,\tilde{I}_0$ fixed, (44) produces a *parameter-free* $\xi(\Xi)$. Then either (i) **predict** μ_n from $\{\widehat{\sigma}_n, \widehat{\Xi}_n\}$ via (31), or (ii) **invert** Ξ_n from the measured μ_n (and $\widehat{\sigma}_n$) and feed Ξ_n back into the moment template to predict ρ_{4n}.

Step 4 (sign discrimination). If the proton calibration prefers $k > 0$ but the neutron moment is negative, then either (a) Ξ_n lies in a shape window where the bracket in (44) is negative, or (b) the neutron occupies $k < 0$ (topology flip). Parity-violating small-$\hat{t}$ measurements (weak slopes) distinguish (a) vs (b) by constraining Ξ_n independently.

B.7 Minimal closed form for quick use

For fast phenomenology, replacing the kernels by the leading thin-torus terms gives

$$\xi(\Xi) \;\approx\; \pi\, k\, \tilde{I}_0\, \frac{(A_\theta - A_\times)\,\Xi \;-\; (A_\phi - A_\times)/\Xi}{A_\phi + A_\theta - 2A_\times}, \tag{47}$$

which is of the intuitive form $\xi(\Xi) = \mathcal{C}_1\,\Xi - \mathcal{C}_2/\Xi$. This *first-principles* expression: (i) is dimensionless, (ii) is finite at $\Xi = 1$, (iii) is linear for $\Xi \gg 1$, and (iv) carries the correct sign structure through k and the geometry bracket.

Connection to the practical ansatz. Matching (47) to the practical template in the main text, $\xi(\Xi) = \xi_0\,(1 + \beta/\Xi^2)/(1 + \gamma/\Xi) \times \mathrm{sgn}(\mathcal{H})$, amounts to the identifications

$$\xi_0 \;\leftrightarrow\; \pi\,|k|\,\tilde{I}_0\,\frac{A_\theta - A_\times}{A_\phi + A_\theta - 2A_\times}, \qquad \frac{\mathcal{C}_2}{\mathcal{C}_1} \;\leftrightarrow\; \frac{A_\phi - A_\times}{A_\theta - A_\times}, \qquad \mathrm{sgn}(\mathcal{H}) = \mathrm{sgn}(k).$$

Thus the ansatz inherits a Canon meaning and can be kept as a fast surrogate until the full kernels are tabulated.

B.8 Summary box

Canon result: The magnetic-moment shape function is

$$\xi(\Xi) \;=\; \pi\, k\, \tilde{I}_0\, \frac{\Xi\,[\ell_{\theta\theta}(\Xi) - \ell_{\phi\theta}(\Xi)] \;-\; \Xi^{-1}[\ell_{\phi\phi}(\Xi) - \ell_{\phi\theta}(\Xi)]}{\ell_{\phi\phi}(\Xi) + \ell_{\theta\theta}(\Xi) - 2\ell_{\phi\theta}(\Xi)},$$

with geometry kernels $\ell_{..}(\Xi)$ defined by A_u Green-kernel integrals on the torus. $\tilde{I}_0$ and the helicity integer k are fixed on the proton magnetic sector once, then reused to *predict* or *invert* the neutron. The neutron's negative moment emerges either from a helicity flip $k \to -k$ or from the bracket changing sign at the neutron's Ξ.

C Kernel cookbook: geometry, kernels, and practical tabulation

This appendix gives explicit Canon/QMU formulas for the geometry kernels $\ell_{\phi\phi}(\Xi)$, $\ell_{\theta\theta}(\Xi)$, and $\ell_{\phi\theta}(\Xi)$ appearing in the quadratic energy (36) and the Canon shape function (44). Everything is dimensionless and SI-free.

C.1 Torus geometry and surface calculus (QMU variables)

We parameterize the thin torus by $(\theta, \phi) \in [0, 2\pi) \times [0, 2\pi)$. Let $\mathcal{R} \equiv R/\lambda_C$, $\nabla \equiv r/\lambda_C$, and $\Xi \equiv \mathcal{R}/\nabla \geq 1$, with $\sigma = \mathcal{R}\,\nabla$ the leng^2 invariant.

Embedding and metric.

$$\boldsymbol{r}(\theta,\phi) = \lambda_C\Big[(\mathcal{R}+\nabla\cos\theta)\,\cos\phi,\ (\mathcal{R}+\nabla\cos\theta)\,\sin\phi,\ \nabla\sin\theta\Big], \tag{48}$$

$$\boldsymbol{r}_\theta = \partial_\theta\boldsymbol{r} = \lambda_C\big[-\nabla\sin\theta\cos\phi,\ -\nabla\sin\theta\sin\phi,\ \nabla\cos\theta\big], \tag{49}$$

$$\boldsymbol{r}_\phi = \partial_\phi\boldsymbol{r} = \lambda_C\big[-(\mathcal{R}+\nabla\cos\theta)\sin\phi,\ (\mathcal{R}+\nabla\cos\theta)\cos\phi,\ 0\big], \tag{50}$$

$$g_{\theta\theta} = \boldsymbol{r}_\theta\cdot\boldsymbol{r}_\theta = {\lambda_C}^2\nabla^2,\quad g_{\phi\phi} = \boldsymbol{r}_\phi\cdot\boldsymbol{r}_\phi = {\lambda_C}^2(\mathcal{R}+\nabla\cos\theta)^2,\quad g_{\theta\phi} = 0, \tag{51}$$

$$dA = \sqrt{g}\,d\theta\,d\phi = {\lambda_C}^2\,\nabla\,(\mathcal{R}+\nabla\cos\theta)\,d\theta\,d\phi. \tag{52}$$

Orthonormal tangents.

$$\boldsymbol{e}_\theta = \frac{\boldsymbol{r}_\theta}{\|\boldsymbol{r}_\theta\|},\qquad \boldsymbol{e}_\phi = \frac{\boldsymbol{r}_\phi}{\|\boldsymbol{r}_\phi\|},\qquad \|\boldsymbol{r}_\theta\| = \lambda_C\nabla,\quad \|\boldsymbol{r}_\phi\| = \lambda_C(\mathcal{R}+\nabla\cos\theta).$$

C.2 Surface-current basis and normalization

We model *uniform* tangential surface-current densities along the two principal directions:

$$\boldsymbol{K}_\phi(\theta,\phi) = \frac{\tilde{I}_\phi}{2\pi}\,\frac{1}{\lambda_C\,\nabla}\,\boldsymbol{e}_\phi,\qquad \boldsymbol{K}_\theta(\theta,\phi) = \frac{\tilde{I}_\theta}{2\pi}\,\frac{1}{\lambda_C\,(\mathcal{R}+\nabla\cos\theta)}\,\boldsymbol{e}_\theta. \tag{53}$$

Here $\tilde{I}_{\phi,\theta}$ are *dimensionless* currents $\tilde{I}_\alpha \equiv I_\alpha/(e{X\,\max}^2 F_q)$, so that all energies below are dimensionless. The prefactors ensure that $\int K_\phi\,\|\boldsymbol{r}_\phi\|\,d\phi/(2\pi) = \tilde{I}_\phi$ and $\int K_\theta\,\|\boldsymbol{r}_\theta\|\,d\theta/(2\pi) = \tilde{I}_\theta$.

C.3 A_u Green kernel and quadratic energy

Let $\mathcal{G}(u)$ be the *dimensionless* A_u vector-potential Green kernel as a function of the dimensionless separation

$$u \;=\; \frac{\|\boldsymbol{r}(\theta,\phi)-\boldsymbol{r}(\theta',\phi')\|}{\lambda_C}.$$

Examples used for tests (pick one and hold fixed across analyses):

$$\text{Coulomb-like:}\ \ \mathcal{G}(u) = \frac{1}{4\pi\,u},\qquad \text{Yukawa-like:}\ \ \mathcal{G}_\zeta(u) = \frac{e^{-\zeta u}}{4\pi\,u},\quad \zeta>0.$$

The *dimensionless* magnetic self-energy of a surface current $\boldsymbol{K}$ is

$$\mathcal{U}[\boldsymbol{K}] = \frac{1}{2}\iint\Big(\boldsymbol{K}(\theta,\phi)\cdot\boldsymbol{K}(\theta',\phi')\Big)\,\mathcal{G}\Big(\frac{\|\boldsymbol{r}-\boldsymbol{r}'\|}{\lambda_C}\Big)\,\frac{dA\,dA'}{{\lambda_C}^2}. \tag{54}$$

Inserting the basis currents (53) and integrating defines the kernels $\ell_{\alpha\beta}(\Xi)$ through $\mathcal{U} = \frac{1}{2}(\ell_{\phi\phi}\tilde{I}_\phi^2 + \ell_{\theta\theta}\tilde{I}_\theta^2 + 2\ell_{\phi\theta}\tilde{I}_\phi\tilde{I}_\theta)$.

C.4 Explicit kernel integrals (dimensionless, QMU)

Write $C(\theta) \equiv \mathcal{R}+\nabla\cos\theta = \nabla(\Xi+\cos\theta)$ and similarly $C'(\theta')$. Define the dimensionless chord distance

$$\begin{aligned} u^2(\theta,\phi;\theta',\phi') &= \frac{\|\boldsymbol{r}-\boldsymbol{r}'\|^2}{{\lambda_C}^2} = \big[C(\theta)\cos\phi - C'(\theta')\cos\phi'\big]^2 + \big[C(\theta)\sin\phi - C'(\theta')\sin\phi'\big]^2 \\ &\quad + \big[\nabla\sin\theta - \nabla\sin\theta'\big]^2 \\ &= C(\theta)^2 + C'(\theta')^2 - 2\,C(\theta)C'(\theta')\cos(\phi-\phi') + \nabla^2(\sin\theta-\sin\theta')^2. \end{aligned} \tag{55}$$

The area elements are $dA = {\lambda_C}^2\,\nabla\,C(\theta)\,d\theta\,d\phi$ and similarly for dA'.

(i) Toroidal–toroidal kernel $\ell_{\phi\phi}(\Xi)$.

$$\ell_{\phi\phi}(\Xi) = \frac{1}{(2\pi)^2}\int_0^{2\pi}\!\!\int_0^{2\pi}\!\!\int_0^{2\pi}\!\!\int_0^{2\pi} \frac{1}{\nabla^2}\,\underbrace{(\boldsymbol{e}_\phi\cdot\boldsymbol{e}_{\phi'})}_{\cos(\phi-\phi')}\,\mathcal{G}\big(u(\theta,\phi;\theta',\phi')\big)\,\nabla C\,\nabla C'\,d\theta\,d\phi\,d\theta'\,d\phi'$$
$$= \frac{1}{(2\pi)^2}\int d\theta\,d\theta'\,d\phi\,d\phi'\,\cos(\phi-\phi')\,\mathcal{G}(u)\,C(\theta)C(\theta'). \tag{56}$$

Using symmetry, one angle can be reduced by setting $\varphi \equiv \phi - \phi'$ and integrating ϕ' trivially (producing a 2π factor).

(ii) Poloidal–poloidal kernel $\ell_{\theta\theta}(\Xi)$.

$$\ell_{\theta\theta}(\Xi) = \frac{1}{(2\pi)^2}\iint \frac{1}{C\,C'}\,\underbrace{(\boldsymbol{e}_\theta\cdot\boldsymbol{e}_{\theta'})}_{\cos(\theta-\theta')+\sin(\theta)\sin(\theta')\cos(\phi-\phi')}\,\mathcal{G}(u)\,CC'\,d\theta\,d\phi\,d\theta'\,d\phi'$$
$$= \frac{1}{(2\pi)^2}\iint \big(\cos(\theta-\theta') + \sin\theta\sin\theta'\cos(\phi-\phi')\big)\,\mathcal{G}(u)\,d\theta\,d\phi\,d\theta'\,d\phi'. \tag{57}$$

Here the (CC') factors from the area elements cancel the normalization factors from the currents.

(iii) Mixed kernel $\ell_{\phi\theta}(\Xi)$.

$$\ell_{\phi\theta}(\Xi) = \frac{1}{(2\pi)^2}\iint \frac{1}{\nabla\,C'}\,\underbrace{(\boldsymbol{e}_\phi\cdot\boldsymbol{e}_{\theta'})}_{\sin(\phi-\phi')\sin\theta'}\,\mathcal{G}(u)\,\nabla C\,C'd\theta\,d\phi\,d\theta'\,d\phi'$$
$$= \frac{1}{(2\pi)^2}\iint \sin(\phi-\phi')\,\sin\theta'\,\mathcal{G}(u)\,C(\theta)\,d\theta\,d\phi\,d\theta'\,d\phi'. \tag{58}$$

The explicit dot product simplifies to a factor $\sin(\phi-\phi')\,\sin\theta'$ in the orthonormal basis.

Practical symmetry reductions. Use $\varphi = \phi - \phi'$ and integrate ϕ' to remove one angle:

$$\iint_{[0,2\pi]^2} F(\phi-\phi')\,d\phi\,d\phi' = 2\pi\int_0^{2\pi} F(\varphi)\,d\varphi.$$

All kernels then become triple integrals over (θ,θ',φ).

C.5 Thin-surface regularization and convergence

The kernels are finite for $\Xi \geq 1$ with the Coulomb-like $\mathcal{G}(u) = 1/(4\pi u)$ once the torus self-interaction is interpreted in the principal-value (PV) sense. Numerically:

- Subtract–add a local singular piece: replace $\mathcal{G}(u) \to \mathcal{G}(u) - \mathcal{G}_{\rm loc}(u)$ inside the integral and add back the analytic $\int \mathcal{G}_{\rm loc}$ piece.
- A simple and effective local kernel is $\mathcal{G}_{\rm loc}(u) = 1/(4\pi\sqrt{u^2+\varepsilon^2})$ with $\varepsilon \sim 10^{-4}$–10^{-3}; verify ε-independence of $\ell_{..}$ in the limit.
- Alternatively, adopt the Yukawa-like $\mathcal{G}_\zeta$ with small ζ as an IR/UV regulator and take $\zeta \to 0^+$ after tabulation checks.

C.6 Numerical quadrature (recommended pipeline)

1. **Variable changes.** Use $\theta = \pi(2x-1)$, $\theta' = \pi(2y-1)$, $\varphi = 2\pi z$ with $x, y, z \in [0,1]$.
2. **Quadrature.** Gauss–Legendre in x, y (order $N_\theta \sim 64$–128) and periodic trapezoid in z (order $N_\varphi \sim 256$–512).
3. **Caching.** Precompute $C(\theta), \sin\theta, \cos\theta$ grids; reuse in all three kernels.
4. **Symmetry.** Exploit even/odd symmetries in φ ($\cos\varphi$, $\sin\varphi$) to halve the grid and reduce cancellation error.
5. **Validation.** Check (i) positivity: $\ell_{\phi\phi}, \ell_{\theta\theta} > 0$; (ii) convexity: $\Delta(\Xi) = \ell_{\phi\phi} + \ell_{\theta\theta} - 2\ell_{\phi\theta} > 0$; (iii) smoothness vs Ξ.
6. **Asymptotics.** Fit $\ell_{..}(\Xi)$ to $A \ln \Xi + B$ for $\Xi \gtrsim 5$ and verify consistency with the Appendix-B asymptotics.
7. **Spline.** Store monotone cubic splines of $\ell_{..}(\Xi)$ over $\Xi \in [1, 10]$ (or desired range).

C.7 Closed-form thin-torus check (sanity test)

For $\Xi \gg 1$ and Coulomb-like $\mathcal{G}$, the torus approaches a circular loop of radius $\mathcal{R}$ with a co-axial thin filament. Then

$$\ell_{\phi\phi}(\Xi) \sim A_\phi \ln \Xi + B_\phi, \quad \ell_{\theta\theta}(\Xi) \sim A_\theta \ln \Xi + B_\theta, \quad \ell_{\phi\theta}(\Xi) \sim A_\times + o(1),$$

with $A_\phi \approx A_\theta$ and $A_\times$ a constant. Plugging these into (44) reproduces the linear asymptote $\xi(\Xi) \sim \mathcal{C}_1 \Xi - \mathcal{C}_2/\Xi$ given in (47).

C.8 End-to-end recipe (one-time computation)

1. Choose and *fix* the A_u kernel $\mathcal{G}$ (Coulomb-like vs Yukawa-like) for the entire analysis program.
2. Tabulate $\ell_{\phi\phi}, \ell_{\theta\theta}, \ell_{\phi\theta}$ on a grid of Ξ with the quadrature above; publish the tables/splines as a QMU resource.
3. Calibrate $k\,\tilde{I}_0$ on the proton magnetic sector using $\{\widehat{\sigma}_p, \widehat{\Xi}_p, \mu_p\}$ and (44).
4. With $k\,\tilde{I}_0$ fixed, *predict* or *invert* the neutron geometry/moment as in Appendix B, then propagate to ρ_{4n} via (10).

C.9 Minimal pseudo-code (dimensionless)

```
for Xi in Xi_grid:
  R = Xi * r
  # Choose r=1 without loss of generality; all results depend on Xi only.
  # Precompute theta, theta', varphi grids and C = R + r*cos(theta)
  lpp = ltt = lpt = 0
  for theta in grid_theta:
    C  = R + cos(theta)
    sT = sin(theta)
    for theta_p in grid_theta:
```

```
    Cp  = R + cos(theta_p)
    sTp = sin(theta_p)
    for varphi in grid_varphi:
      # chord distance u (dimensionless)
      u2 = C*C + Cp*Cp - 2*C*Cp*cos(varphi) + (sT - sTp)*(sT - sTp)
      u  = sqrt(u2)
      G  = kernel(u)  # e.g. 1/(4*pi*u) with regulator near u=0
      # contributions
      lpp += cos(varphi) * G * C * Cp
      ltt += (cos(theta - theta_p) + sT*sTp*cos(varphi)) * G
      lpt += sin(varphi) * sTp * G * C
# normalize by (2*pi)^2 and weights
lpp /= (2*pi)^2; ltt /= (2*pi)^2; lpt /= (2*pi)^2
save(Xi, lpp, ltt, lpt)
```

Note. We set $r = 1$ in the pseudo-code because all kernels depend only on $\Xi = R/r$ after factoring λ_C; this is the QMU scaling. When using the kernels in (44), supply the physical Ξ inferred from data.

C.10 Deliverables for experimental teams

Publish (i) the kernel tables $\ell_{\cdot\cdot}(\Xi)$ with interpolation code, (ii) the calibrated constant $k\,\tilde{I}_0$ (with uncertainty), and (iii) a short example that takes (σ_X, Ξ_X) to μ_X via (31)+(44), and back again (inversion). All quantities remain in Canon/QMU throughout.

References and Ledger Resources

- Aether Physics Model (APM) constants and units in QMU, including $p = e^2/(8\pi\, {e_{pmax}}^2)$, $n = e^2/(8\pi\, {e_{nmax}}^2)$: sota.aetherwizard.com/constants#fine_structure.
- APM angular-momentum geometry and Aether unit background: sota.aetherwizard.com/angular-momentum.